

SCIENTIFIC REPORTS



OPEN

Development of an *in-vivo* active reversible butyrylcholinesterase inhibitor

Received: 15 June 2016
Accepted: 21 November 2016
Published: 21 December 2016

Urban Košak¹, Boris Brus¹, Damijan Knez¹, Roman Šink¹, Simon Žakelj¹, Jurij Trontelj¹, Anja Pišlar¹, Jasna Šlenc¹, Martina Gobec¹, Marko Živin², Larisa Tratnjek², Martina Perše³, Kinga Sałat⁴, Adrian Podkowa⁴, Barbara Filipek⁴, Florian Nachon⁵, Xavier Brazzolotto⁵, Anna Więckowska⁴, Barbara Malawska⁴, Jure Stojan⁶, Irena Mlinarič Raščan¹, Janko Kos¹, Nicolas Coquelle^{7,8,9}, Jacques-Philippe Colletier^{7,8,9} & Stanislav Gobec¹

Alzheimer's disease (AD) is characterized by severe basal forebrain cholinergic deficit, which results in progressive and chronic deterioration of memory and cognitive functions. Similar to acetylcholinesterase, butyrylcholinesterase (BChE) contributes to the termination of cholinergic neurotransmission. Its enzymatic activity increases with the disease progression, thus classifying BChE as a viable therapeutic target in advanced AD. Potent, selective and reversible human BChE inhibitors were developed. The solved crystal structure of human BChE in complex with the most potent inhibitor reveals its binding mode and provides the molecular basis of its low nanomolar potency. Additionally, this compound is noncytotoxic and has neuroprotective properties. Furthermore, this inhibitor moderately crosses the blood-brain barrier and improves memory, cognitive functions and learning abilities of mice in a model of the cholinergic deficit that characterizes AD, without producing acute cholinergic adverse effects. Our study provides an advanced lead compound for developing drugs for alleviating symptoms caused by cholinergic hypofunction in advanced AD.

Alzheimer's disease (AD) is a complex neurodegenerative disorder that is characterized by progressive and chronic deterioration of memory and other cognitive functions. This disease leads to death within 3 years to 9 years after diagnosis, and as the leading cause of dementia, it affects 44 million people worldwide¹.

Even though the etiology of AD is very complex, several conditions are known to participate in the associated neurodegeneration. Accumulation of amyloid β peptide (A β) deposits^{2,3}, abnormal modification and accumulation of the protein tau⁴ accompanied with oxidative stress in the brain lead to synaptic dysfunction and neurodegeneration¹. This most severely affects the cholinergic system⁵ and results in a decrease in the levels of the neurotransmitter acetylcholine (ACh)⁶, which in turn produces memory and cognitive deficits⁷, characteristic for patients with AD. Cholinergic neurotransmission in the brain is terminated by the hydrolysis of ACh, which is catalyzed by two cholinesterases (ChEs): acetylcholinesterase (AChE) and butyrylcholinesterase (BChE)⁸. In the brain of healthy adults, AChE accounts for 80% of the ChE activity, with BChE accounting for the remainder⁹.

As long as AD cannot be prevented, symptomatic treatment is essential. Three out of the four approved drugs for treatment of patients with AD are ChE inhibitors: the selective reversible AChE inhibitors donepezil¹⁰ and galantamine¹¹, and the pseudo-irreversible dual ChE inhibitor rivastigmine¹² (Fig. 1a). These drugs exploit ChE inhibition to alleviate the symptoms of AD, or to temporarily slow down its progression, by restoring the cholinergic activity in the brain. However, inhibition of AChE in the peripheral nervous system and the parasympathetic autonomic nervous system represents the basis for the adverse side effects (e.g., nausea, vomiting, diarrhea,

¹Faculty of Pharmacy, University of Ljubljana, Aškerčeva 7, 1000 Ljubljana, Slovenia. ²Institute of Pathological Physiology, Faculty of Medicine, University of Ljubljana, Vrazov trg 2, 1000 Ljubljana, Slovenia. ³Institute of Pathology, Faculty of Medicine, University of Ljubljana, Korytkova 2, 1000 Ljubljana, Slovenia. ⁴Faculty of Pharmacy, Jagiellonian University, Medyczna 9 St., 30-688 Krakow, Poland. ⁵Institut de Recherche Biomédicale des Armées, 91223 Brétigny sur Orge, France. ⁶Institute of Biochemistry, Faculty of Medicine, University of Ljubljana, Vrazov trg 2, 1000 Ljubljana, Slovenia. ⁷University Grenoble Alpes, IBS, F-38044 Grenoble, France. ⁸CNRS, IBS, F-38044 Grenoble, France. ⁹CEA, IBS, F-38044 Grenoble, France. Correspondence and requests for materials should be addressed to S.G. (email: stanislav.gobec@ffa.uni-lj.si) or J.-P.C. (email: jacques-Philippe.Colletier@ibs.fr)

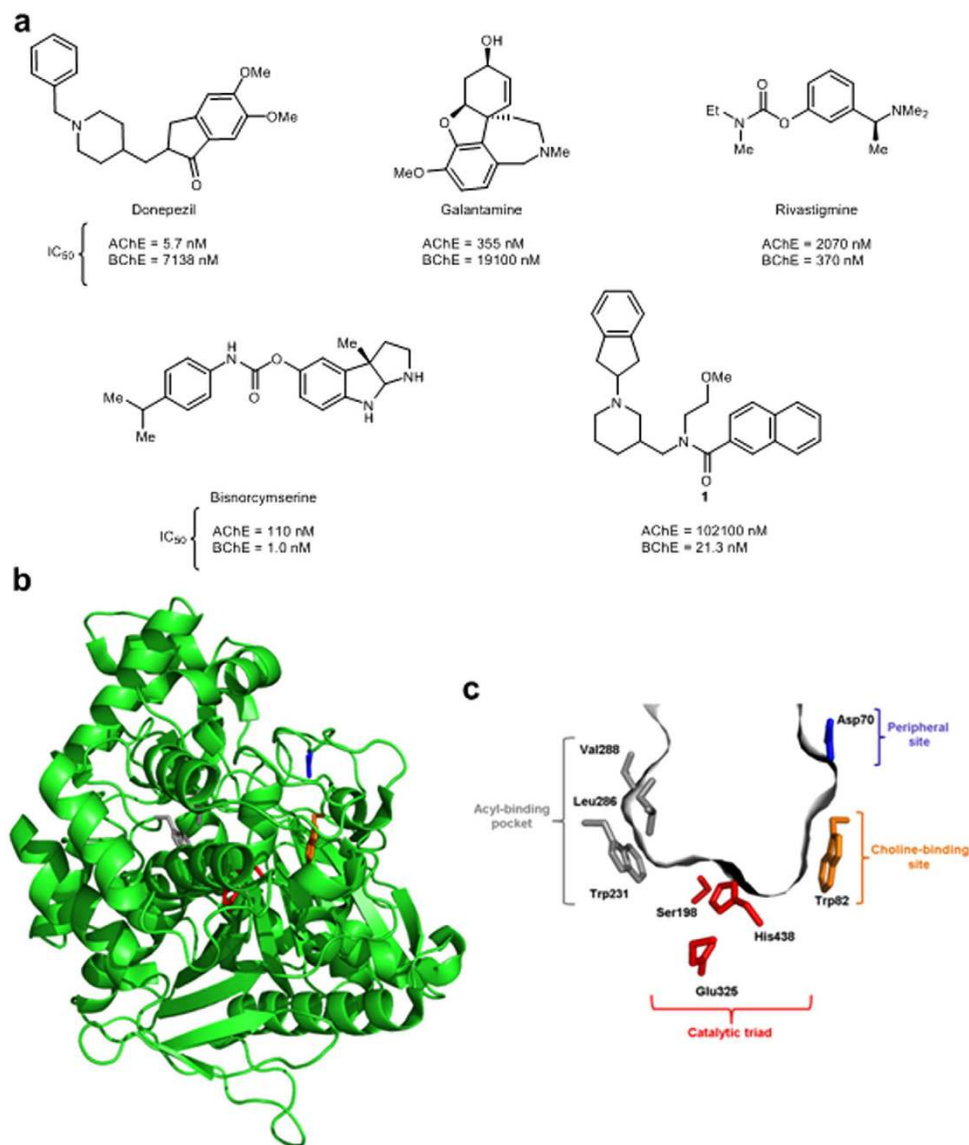


Figure 1. ChE inhibitors and structures of huBChE and its active site gorge. (a) Structures and IC_{50} values against the ChEs of the currently approved drugs for the treatment of AD symptoms that exploit ChE inhibition (donepezil, galantamine, rivastigmine) and selective huBChE inhibitors (bisnorcymserine and compound 1). (b) The overall structure of huBChE (PDB code 4TPK) shown as a green cartoon with the key amino acids of the active site shown as sticks. (c) The active site gorge of huBChE shown as a gray surface. The principal contributors to the peripheral site (Asp70; blue), the choline-binding site (Trp82; orange), the catalytic triad (Ser198, Glu325, His438; red), and the acyl-binding pocket (Trp231, Leu286, Val288; gray) are shown as sticks.

tremors¹³, and also limits the doses¹⁴ of these drugs that can be administered. Additionally, the clinical efficacy of this drug class is mostly limited to mild and moderate stages of AD^{15,16}.

The assumed co-regulatory function of BChE in termination of cholinergic neurotransmission in the healthy brain changes in brains of patients with progressive AD. In specific brain regions of these patients enzymatic activity of BChE is increased⁷. Increased BChE activity⁷ in addition to reduced expression of neuronal AChE in advanced AD⁹, findings that AChE knockout mice are viable and develop a primitive cholinergic neuronal network with BChE acting as a surrogate for AChE and taking over the hydrolysis of ACh in the brain¹⁷, along with the fact that BChE knockout mice show no physiological disadvantages¹⁸, have led to the hypothesis that BChE takes over the ChE activity in advanced AD, and thus needs to be inhibited to restore the brain levels of ACh¹⁷. In line with this hypothesis, in aged rats, selective inhibition of BChE with cymserine analogs raises ACh levels in the brain and improves cognitive performance¹⁹ without any adverse parasympathetic side effects¹³. Altogether, these data suggest that BChE is a potential therapeutic target for restoring ACh levels in the brain and thus improving cognitive impairment, while also minimizing adverse effects in patients with progressive AD.

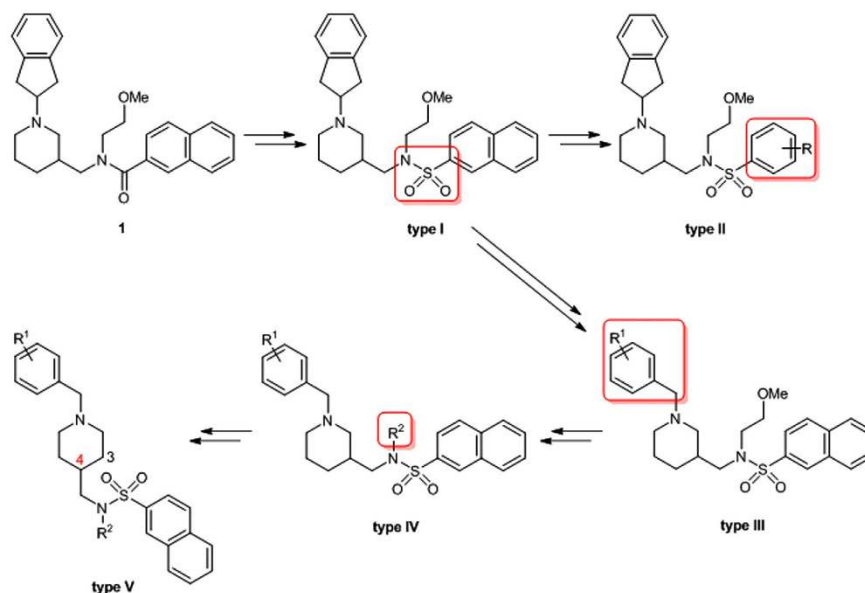


Figure 2. Design of sulfonamide analogs of hit compound 1. The modifications introduced during each design step are indicated in red.

Although a number of structurally diverse selective reversible and pseudo-irreversible BChE inhibitors have been reported^{19–25}, cymserine analogs are the only BChE inhibitors with reported *in-vivo* activity¹⁹, and one of them has successfully advanced to Phase I clinical trials: bisnorcymserine (Fig. 1a). Cymserine analogs are pseudo-irreversible carbamate inhibitors, the mechanism of action of which involves a rapid initial covalent reaction between their carbamate carbonyl group and the catalytic serine in the active site of ChEs (carbamoylation), followed by a slower regeneration (decarbamylation) of the active enzyme²⁶. Pseudo-irreversible inhibitors are thus reversible covalent inhibitors, and since they derive their activity by forming a covalent bond with their target, concerns remain over their potential nonspecific or off-target reactivity-based toxicities^{27,28}. *In-vivo* active selective reversible BChE inhibitors are thus highly desirable not only as potential clinical candidates for improving memory and cognitive deficits in patients with progressive AD, but also as molecular tools for studying the potential of BChE as a therapeutic target. The structures of human BChE (huBChE) and its active site gorge are shown in Fig. 1b,c.

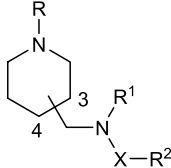
Recently, a novel piperidine-3-ylmethanamine-based selective huBChE inhibitor **1** was reported (Fig. 1a) that shows reversible, slow-tight binding inhibition of huBChE with low nanomolar IC_{50} ²⁹. This inhibitor was used here as the starting point for the design, synthesis, and biochemical evaluation of a comprehensive series of sulfonamides. The most potent of these, compound **2**, shows selective reversible nanomolar huBChE inhibition with a new binding mode, as revealed by the crystal structure of its complex with huBChE. Furthermore, compound **2** improves memory, cognitive functions, and learning abilities of mice in a model that mimics the symptoms of AD caused by cholinergic hypofunction, without producing acute cholinergic adverse effects.

Results

Design and synthesis of inhibitors. Our quest for novel sulfonamide BChE inhibitors began before the crystal structure of hit compound **1** in complex with huBChE was solved. Thus, the initial design efforts were based solely on the chemical structure of hit compound **1**, which made it imperative that this design and synthesis yielded compounds with drug-like properties³⁰ and good synthetic tractability.

The bioisosteric replacement of a carboxamide with a sulfonamide group is a common design strategy in medicinal chemistry that has been used to improve biological activity, bioavailability, and metabolic stability of drug candidates³¹. Accordingly, the **type I** inhibitor was designed by replacing the carboxamide group of compound **1** with a sulfonamide group. Additional types of inhibitors were designed to study the effects of these structural modifications on the inhibitory potencies against huBChE. The naphthalene moiety was truncated and replaced with various substituted phenyl rings (**type II** inhibitors). Analogously, the 2,3-dihydro-1*H*-inden moiety was replaced with various benzyl rings (**type III** inhibitors), and the importance of the *N*-alkyl chain on the sulfonamide nitrogen of these inhibitors was studied by its removal or replacement with linear alkyl substituents (**type IV** inhibitors). Finally, 1,4-disubstituted piperidine derivatives (**type V** inhibitors) were designed to determine the effects of a piperidine ring disubstitution pattern (Fig. 2). In conjunction with this, a synthesis route was planned that provided the simple and rapid generation of new inhibitors. Details regarding the synthesis of all of the 41 inhibitors are given in Supplementary Figures 1 to 5.

***In-vitro* ChE inhibition and structure–activity relationships.** The inhibitory potencies against huBChE and murine AChE (mAChE) were determined for all of these synthesized compounds using the method of Ellman³². mAChE was chosen as the surrogate for huAChE on the basis that the distribution of the amino-acid residues along the active site gorge of these two enzymes is strictly conserved³³. Table 1 gives the inhibitory



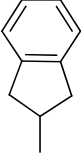
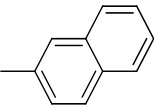
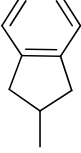
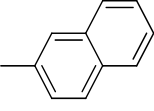
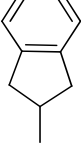
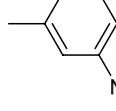
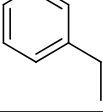
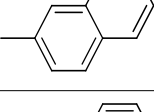
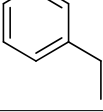
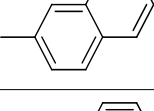
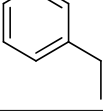
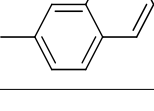
Inhibitor type	Cn ^a	Pds ^b	X	R	R ¹	R ²	IC ₅₀ ± SEM (nM)	%RA ^c at 10 μM ± SEM	IC ₅₀ (nM) or %RA ^{c,d} at 10 μM ± SEM
							huBChE		mAChE
Initial hit	1	1,3	CO		(CH ₂) ₂ OMe		21 ± 2	0.95% ± 0.56%	102100 ± 2500 nM
Type I	3	1,3	SO ₂		(CH ₂) ₂ OMe		53 ± 4	1.47% ± 1.54%	72% ± 1%
Type II	4	1,3	SO ₂		(CH ₂) ₂ OMe		197 ± 8	2.34% ± 0.13%	90% ± 0.003%
Type III	2	1,3	SO ₂		(CH ₂) ₂ OMe		4.9 ± 0.3	0.40% ± 0.77%	97% ± 2%
Type IV	5	1,3	SO ₂		(CH ₂) ₃ OMe		14.4 ± 0.8	0.71% ± 0.66%	95% ± 5%
Type V	6	1,4	SO ₂		(CH ₂) ₃ OMe		19.3 ± 3.7	0.93% ± 0.27%	95% ± 4%

Table 1. Inhibitory potencies and structures of hit compound 1 and the most potent of the type I to V inhibitors. ^aCn = compound number. ^bPds = piperidine disubstitution pattern. ^cRA = residual activity. ^d%RA > 75% was considered as no inhibition.

potencies (i.e., IC₅₀ values, % residual activities [RAs]) and structures of the most potent of these **type I–V** inhibitors (**2–6**), and for a comparison, those of initial hit compound **1**. The complete list of all 41 sulfonamides is given in Supplementary Table 1. Briefly, these IC₅₀ values against huBChE ranged from 4.9 nM to 8270 nM, and all of these compounds showed significant selectivity towards huBChE over mAChE. Bioisosteric replacement of carboxamide in hit compound **1** with sulfonamide in the **type I** inhibitor (compound **3**) slightly reduced the inhibitory potency against huBChE. When the naphthalene ring of the **type I** inhibitor compound **3** was replaced with substituted phenyl rings (e.g., **type II** inhibitors), the inhibitory potencies against huBChE dropped significantly. The naphthalene ring was therefore retained, and the left-hand side of the **type I** inhibitor structure illustrated in Table 1 was modified further. The replacement of 2,3-dihydro-1*H*-inden ring with benzyl groups yielded **type III** inhibitors, among which compound **2** was the most potent inhibitor of the series, with an IC₅₀ of 4.9 nM against huBChE. The **type IV** inhibitors revealed that variations in the *N*-alkyl substituent on the sulfonamide nitrogen were permitted for maintained inhibitory potency against huBChE, although its removal was not (Table 1 and Supplementary Table 1). Additionally, introduction of substituents to the benzyl and naphthalene rings of **type III** and **type IV** inhibitors were not tolerated for inhibitory activity against huBChE (Supplementary Table 1). **Type V** inhibitors showed that 1,3 disubstituted piperidines were more potent huBChE inhibitors than their 1,4 disubstituted counterparts (Table 1 and Supplementary Table 1).

Chiral HPLC resolution and kinetic evaluation of compound 2. Compound **2** was resolved into its pure enantiomers using semi-preparative reversed-phase chiral HPLC (Fig. 3a and Supplementary Methods).

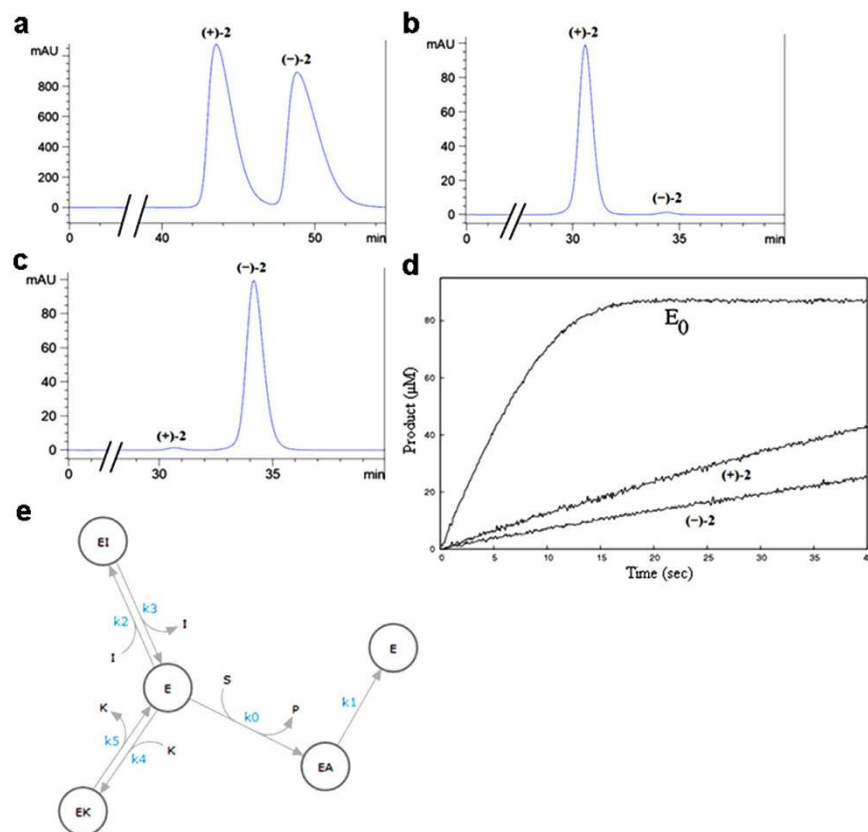


Figure 3. Chiral HPLC resolution of racemic compound (\pm)-2 into pure enantiomers, and their kinetic evaluation. (a) Semi-preparative reversed-phase HPLC of racemic compound (\pm)-2 (Supplementary Methods [method A; 254 nm]). (b) Analytical reversed-phase chiral HPLC of (+)-2 (Supplementary Methods [method B; 254 nm]). (c) Analytical reversed-phase chiral HPLC of (-)-2 (Supplementary Methods [method B; 254 nm]). (d) Progress curves for hydrolysis of 44 μ M butyrylthiocholine iodide by huBChE in the absence (E_0) and presence of 50 nM of each pure enantiomer of compound 2 (as indicated). Data were obtained using a stopped-flow apparatus. (e) A competitive single-step inhibition mechanism with fast association (high k_2 , k_4) for each pure enantiomer fully reproduced the progress curves obtained. S, substrate; P, product; E, enzyme; EA, acylated enzyme; I, (-)-2; K, (+)-2; k_0 – k_5 , kinetic constants.

The optical purities of the enantiomers were determined by measurement of the optical rotation (Supplementary Methods) and by determination of the enantiomeric excess (e.e.) using analytical reversed-phased chiral HPLC (Fig. 3b,c, and Supplementary Methods). Both of these enantiomers were obtained with e.e. 97%. The inhibitory potencies of these separated enantiomers were evaluated, whereby enantiomer (-)-2 had an IC_{50} of 4.5 nM and was a 3.4-fold more potent huBChE inhibitor than the diastereomer (+)-2 ($IC_{50} = 15.3$ nM). Given the affinity of compound (-)-2 for its target enzyme huBChE, standard methods for K_i determination (e.g., Lineweaver-Burk plots) or approximation (e.g., Cheng-Prusoff equations) are inappropriate, as i) the target enzyme huBChE does not obey the typical Michaelis-Menten kinetics³⁴ and ii) the concentration of the inhibitor is approaching the enzyme concentration (50 and 8.2 nM, respectively) in the assay system. This situation is referred to as tight binding inhibition. Given these facts, in order to obtain the true affinity of the pure enantiomers of compound 2, the enzyme kinetics experiments were carried out in a stopped-flow apparatus, according to Copeland's guidelines for evaluation of tight-binding inhibitors³⁵. The full progress curves of product formation were followed in the absence and presence of each pure enantiomer of 2 (Fig. 3d). Of note, a high enzyme concentration was used in order to investigate the time-dependent inhibition and to reach the plateau of the reaction, which allowed precise quantification of the substrate concentration. No curvature in the initial phase of the inhibited enzyme reaction was observed, indicating that the compound 2 does not display slow-binding inhibition. The curves were analyzed simultaneously using the ENZO application³⁶. Several inhibition mechanisms were tested, and the single-step competitive mechanism allowed full reproduction of the progress curves (Fig. 3e). The inhibition constants of 1.29 nM and 2.01 nM were determined for the enantiomers (-)-2 and (+)-2, respectively. The determined rates and the calculated dissociation constants for each of these enantiomers, along with the K_m and k_{cat} values for butyrylthiocholine iodide, are given in Supplementary Table 2. The low degree of stereoselective inhibition provided an advantage for compound 2, as it enabled the use of the readily available synthetic racemic mixture in further *in-vitro* and *in-vivo* studies.

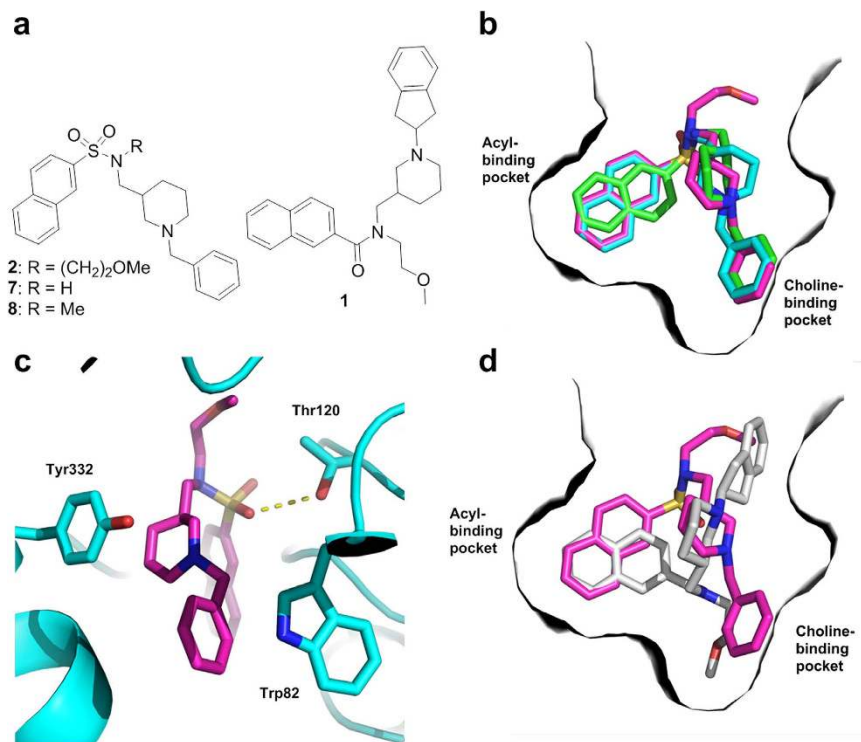


Figure 4. Crystal structures of huBChE in complex with compounds 2, 7, and 8. (a) Two-dimensional structures of the co-crystallized sulfonamides 2, 7, and 8 and hit compound 1. (b) Alignment of crystal structures of compounds 2 (purple), 7 (green), and 8 (cyan) in their complexes with huBChE (gray surface). These inhibitors fully occupy the acyl-binding and choline-binding pockets with their naphthalene and benzyl moieties, respectively. (c) The polar interactions of compound 2 (purple sticks) with the amino-acid residues of the huBChE active site (blue) contribute significantly to the binding affinity. The observed H-bond between Thr120 and the sulfonamide moiety is shown as yellow dashes (distance, 3.1 Å). Compound 2 forms cation- π and π - π aromatic interactions with Tyr332 and Trp82, respectively. (d) Alignment of crystal structures of compound 2 (purple) and hit compound 1 (white) in their complexes with huBChE (white surface). PDB codes: 5DYW (compound 2), 5DYY (compound 7), and 5DYT (compound 8).

Crystal structures of huBChE in complex with compounds 2, 7, and 8. The crystallographic structures of huBChE in complex with compounds 2 [-(CH₂)₂-OMe], 7 (-H), and 8 (-Me) were solved. These compounds differ only in terms of the presence and nature of their *N*-alkyl group (Fig. 4a), and hence share a similar binding modes for huBChE (Fig. 4b and Supplementary Figure 6). Specifically, the positively charged nitrogen of their piperidine moiety engages in cation- π interaction with the Tyr332 side chain, while the attached benzyl ring fits into a groove contributed by Tyr82, Tyr332, Trp430, and Tyr440 side chains, in the choline-binding pocket. The naphthalene moiety is T-stacked (i.e., π - π interaction) to Trp231 in the acyl-binding pocket, while one of the sulfonamide oxygens forms a H-bond to the hydroxyl oxygen of Thr120 (Fig. 4c and Supplementary Figure 1). The -(CH₂)₂-OMe (compound 2) or methyl (compound 8) side chains point out of the gorge (Fig. 4b). This binding mode was not expected, given that the -(CH₂)₂-OMe side chain of hit compound 1 (Fig. 4a), which served as the scaffold for the design of these sulfonamide inhibitors, is instead oriented toward the choline-binding pocket (Fig. 4d)²⁸. This phenomenon can be explained by the different hydrogen-bonding and geometrical preferences of the carboxamide (compound 1) and sulfonamide (compound 2) groups³⁷. Furthermore, a H-bond is observed between the ether oxygen of compound 2 and a structural water, which is itself H-bonded to Asn68. The position of this oxygen appears to be important for the affinity of compound 2, as the additional methylene group in the *N*-alkyl chain [(CH₂)₃OMe] of compound 5 resulted in a 3-fold higher IC₅₀ against huBChE than for compound 2 (Table 1). As observed already in the complex structure of huBChE with compound 1²⁸, no conformational change is undergone by the enzyme upon binding of compounds 2, 7, and 8. This observation suggests that the active site of huBChE is fairly rigid upon binding and that tailor-made compounds are required to achieve potent huBChE inhibition. The larger binding surface and the greater surface complementarity (Supplementary Table 3) indeed correlate with higher affinity (Supplementary Table 1). The 2mFo-DFc electron density map of compound 2 bound in the active site of huBChE is shown in Supplementary Figure 7. As both the *R* and *S* enantiomers of these sulfonamide inhibitors provided a fit to the electron density maps, all of the inhibitors were assigned to the *R*-enantiomers, on the basis of a possible cation- π interaction between the positively charged nitrogen of the piperidine moiety and the side chain of Tyr332, which is not possible for *S*-enantiomers.

Inhibition of BChE in rat brain slices. To investigate whether compound 2 can efficiently inhibit BChE in an environment that is more similar to *in-vivo* conditions, inhibition of BChE in rat brain slices was performed.

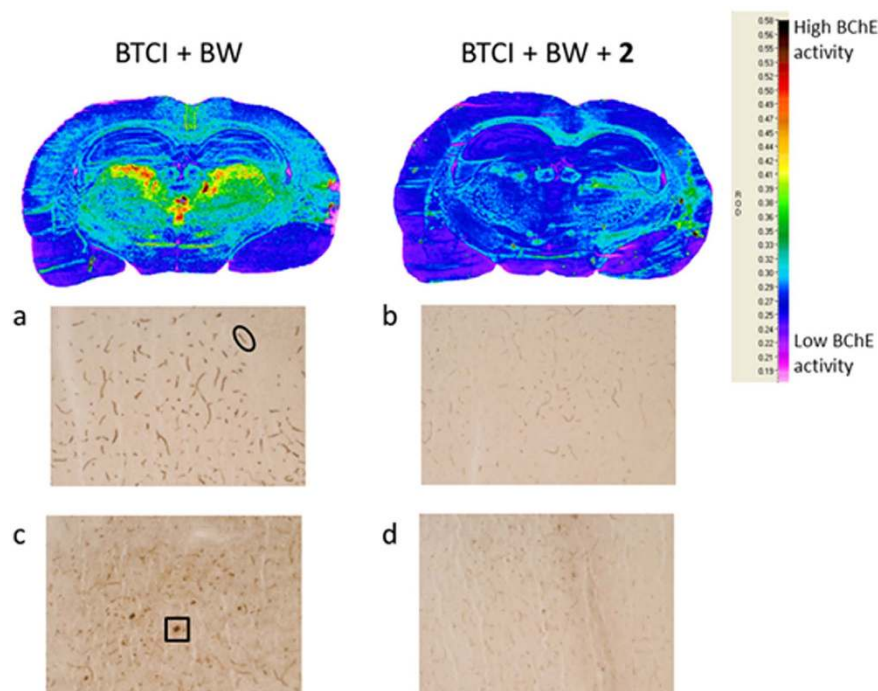


Figure 5. Inhibition of BChE in rat brain slices. Representative coronal section from a rat brain in the region of the thalamus processed for BChE histochemical staining using 4 mM butyrylthiocholine iodide (BTCI), in the absence (left) and presence (right) of 300 μM compound **2**. Here, 10 mM BW-284C51 (BW) was added to completely block AChE activity. Vascular structures in the cortex (black oval highlight) and BChE-rich neurons in the laterodorsal thalamic nucleus (black box highlight) in the absence (a,c) (respectively) and presence (b,d) (respectively) of compound **2**. Magnification, 10 \times . The relative optical density (ROD) scores for the staining intensity for BChE activity are shown on the right.

To detect the regions with the highest BChE activities in the rat brain, these were mapped and processed using a modified Koelle-Karnovsky histochemical method³⁸. The dark brown/black granular BChE reaction product was mainly associated with glial cells, and vascular and neuronal structures. Most of the BChE-positive neurons were in the thalamus, neocortex, and amygdala, while very few were detected in the striatum and hippocampus, which is in agreement with previously published studies^{39,40}. The highest BChE activity was detected in the laterodorsal thalamic nucleus, and the sections containing this region were further used in the inhibition experiments. There was significant reduction in the dark brown/black BChE reaction product that was formed when these sections were incubated with 300 μM compound **2** (Fig. 5).

Cytotoxicity and neuroprotective effects of compound 2. Prior to any *in-vivo* investigations, the cytotoxicity profiles of compound **2** on the human liver cancer HepG2 (Supplementary Figure 8a) and neuroblastoma SH-SY5Y (Supplementary Figure 8b) cell lines were determined. The LD₅₀ value for compound **2** with HepG2 cells was 58.67 μM , and with SH-SY5Y cells, 31.40 μM . These LD₅₀ values were almost 12,000-fold and >6,400-fold greater, respectively, than the concentrations needed to achieve 50% *in-vitro* inhibition of huBChE.

Neurotoxicity induced by A β species (mainly A $\beta_{(1-42)}$) is a contributor to the pathogenesis of neurodegeneration in AD⁴¹. To determine whether compound **2** can protect neuronal cells from toxic A β -species, comparisons were made of the neuronal death induced by A $\beta_{(1-42)}$ in the absence and presence of various concentrations of compound **2**. As shown in Supplementary Figure 8c, treatment of SH-SY5Y cells with 5 μM A $\beta_{(1-42)}$ caused significant toxicity, whereas a clear dose-response neuroprotective effect was observed when the cells were exposed to A $\beta_{(1-42)}$ in the presence of compound **2**. Indeed, at 10 μM , this BChE inhibitor reversed A $\beta_{(1-42)}$ -induced cell death. The neuroprotective effects of compound **2** are independent of A $\beta_{(1-42)}$ aggregation as 10 μM compound **2** did not inhibit A $\beta_{(1-42)}$ aggregation (Supplementary Table 4).

***In-vitro* pharmacokinetics of compound 2.** Since permeability values (P_{app}) of compounds in Caco-2 cells (heterogeneous human epithelial colorectal adenocarcinoma cells) correlate well with *in-vivo* permeation⁴², simple *in-vitro* bidirectional permeability measurements in these cells are used to predict the absorption in humans⁴³. Caco-2 cells are also used to investigate a compounds transport mechanisms⁴³, as they express membrane transport proteins like P-glycoprotein or breast cancer resistance protein (BCRP)⁴⁴, which actively efflux drugs⁴². The P_{app} of compound **2** was determined in both directions, in eliminatory [basolateral-to-apical (B–A)] and absorptive [apical-to-basolateral (A–B)], and the efflux ratio [$P_{\text{app(B-A)}}$ / $P_{\text{app(A-B)}}$] was calculated. The $P_{\text{app(B-A)}}$ of compound **2** (29.1 ± 2.9) $\times 10^{-6}$ cm s⁻¹, was “high” according to the biopharmaceutical classification system of drug permeability since it is comparable to those of antipyrine, naproxen, propranolol and theophylline

previously measured in the same experimental setting in the same laboratory⁴⁵. In the opposite direction the $P_{app(A-B)}$ was $(30.0 \pm 10.7) \times 10^{-6} \text{ cm s}^{-1}$ which results in an efflux ratio (P_{B-A}/P_{A-B}) of 0.97 and demonstrates that compound **2** is not subject to any significant active efflux mechanisms⁴⁶.

10 mM compound **2** was incubated with human blood plasma to determine its plasma protein binding. Equilibrium dialysis showed that compound **2** is 96% protein bound (Supplementary Table 5), which is higher than the threshold of 90%, above which a compound is classified as highly protein bound⁴⁷.

The *in-vitro* metabolic stability was studied by performing incubations of compound **2** in the presence of human blood plasma to determine the plasma half-life and with human cryopreserved hepatocytes (0.7 million viable cells/mL) to determine the intrinsic hepatic metabolic clearance. The plasma metabolic stability and hepatic clearance were estimated by the substrate depletion method. Qualitative aspect of metabolic degradation was performed by metabolite identification using LC-high resolution mass spectrometry (HRMS). We determined that the *in-vitro* half-life of compound **2** in human plasma was >120 min (Supplementary Table 6), while its hepatic metabolism assessed by cryopreserved hepatocytes was more pronounced ($t_{1/2} = 54 \text{ min}$) (Supplementary Table 7). This half-life of compound **2** is comparable to other high extraction ratio reference compounds cleared by CYP enzymes that were used in the metabolic stability experiment as positive controls (Supplementary Table 7). The marked hepatocyte clearance ($18.2 \mu\text{L}/\text{min}/\text{million cells}$) (Supplementary Table 7) of compound **2** is in agreement with the three possible metabolites identified with LC-HRMS: *N*-debenzylated, demethylated, and a demethylated + glucuronide products (Supplementary Figure 9 and Supplementary Table 8).

***In-vivo* blood plasma–brain distribution of compound 2.** Partition into the brain is essential for compounds designed to be active in the central nervous system, and the most reliable evaluation of this crossing of the blood–brain barrier (BBB) by any molecule comes from direct *in-vivo* measurements of the distribution between the blood plasma and the central nervous system⁴². The distribution of compound **2** between the blood plasma and the brain was therefore measured in 3-month-old female Wistar Han rats, using liquid chromatography combined with tandem mass spectrometry (LC-MS/MS) for the analysis. One hour after these rats had an intraperitoneal (IP) injection of 10 mg kg^{-1} compound **2**, or 2 mg kg^{-1} donepezil (positive control), or vehicle (negative control), they were euthanized, and blood samples were collected and the brain tissue was isolated. The methods developed for the preparation of the blood plasma and the brain tissue included homogenization, centrifugation, and solid-phase extraction for preparation of the samples for LC-MS/MS quantification (Methods, Supplementary Methods).

Using a validated UHPLC-MS/MS method (Supplementary Methods), the mean \pm SEM concentration of compound **2** in the brain tissue was determined as $78 \pm 7 \mu\text{g kg}^{-1}$, while that in the blood plasma was $168 \pm 10 \mu\text{g L}^{-1}$. The brain-to-plasma ratio of compound **2** was thus 0.44. This procedure was verified using the donepezil positive control, which provided a brain-to-plasma ratio of 6.3, which is in agreement with previous reports⁴⁸. This lower BBB permeability of compound **2** did not prevent us from carrying out further investigations into this compound. High BBB permeability is essential for acute treatments, e.g., analgesics for acute pain, and it is of lesser importance for chronic administration schedules, e.g., ChE inhibitors for AD, where even compounds with modest permeability can produce significant pharmacological effects⁴².

Among the major reason for limited brain exposure of compounds designed to be active in the central nervous system is their low passive permeability combined with active efflux by membrane transport proteins like P-glycoprotein or breast cancer resistance protein (BCRP) and high molecular weight⁴². The results of permeability measurements with Caco-2 cells show that neither low passive permeability nor active efflux are likely not the reason for the relatively modest brain-to-plasma ratio of compound **2**. This could be due to its molecular weight (453 Da), which is considered borderline high for favorable distribution into the brain⁴².

***In-vivo* activity of compound 2.** *Passive avoidance task.* The first behavioral test performed was the passive avoidance (PA) task, which allows the evaluation of the effects of a drug on fear-motivated contextual memory. This is one of the most frequently used behavioral methods to measure the effects of drug candidates on cognitive abilities in rodents⁴⁹. In the passive avoidance task, better memory performance is determined according to a longer step-through latency in the retention trial (i.e., the testing phase) than in the acquisition trial (i.e., the conditioning phase). Comparison of the retention trial step-through latencies in scopolamine-treated and vehicle-treated mice (23, 178 s, respectively; Fig. 6a) demonstrated the amnesic effect of scopolamine on learning and memory. Administration of compound **2** before scopolamine led to significant prolongation of the step-through latencies at each dose tested (10, 20, 30 mg kg^{-1} , for latencies of 70, 58, 102 s, respectively). Administration of 1 mg kg^{-1} and 2.5 mg kg^{-1} rivastigmine also prolonged the step-through latency (85, 99 s, respectively), while 0.5 mg kg^{-1} rivastigmine was not active (Fig. 6a). As compound **2** was tested *in-vivo* for the first time, and as no effective concentration ranges had been established before, the two further behavioral tests were carried out with 30 mg kg^{-1} compound **2**.

Morris water maze task. The Morris water maze (MWM) task is a hippocampus-dependent spatial learning and memory task that provides insight into long-term memory through decreases in escape latency time, and into cognition through the measure of the overall distance travelled to reach the platform^{50,51}. In this task the time taken to reach the hidden platform (i.e., the escape latency time), the distance travelled, and the mean speed of swimming are recorded for each experimental group. For all of the groups of mice tested, the latency times to reach the platform tended to decrease along with the training, according to characteristic learning curves (Fig. 7b–e). The amnesic effect of scopolamine was seen from day 3, with a statistically significant increase in the distance travelled to reach the platform (vehicle treated, 3.77 m; scopolamine treated, 8.71 m), which was more pronounced on day 5 (1.94, 5.40 m, respectively). Mice treated with scopolamine and compound **2** travelled 5.38 m on day 3, and 1.69 m on day 5, which demonstrated the procognitive effect of compound **2**. In comparison,

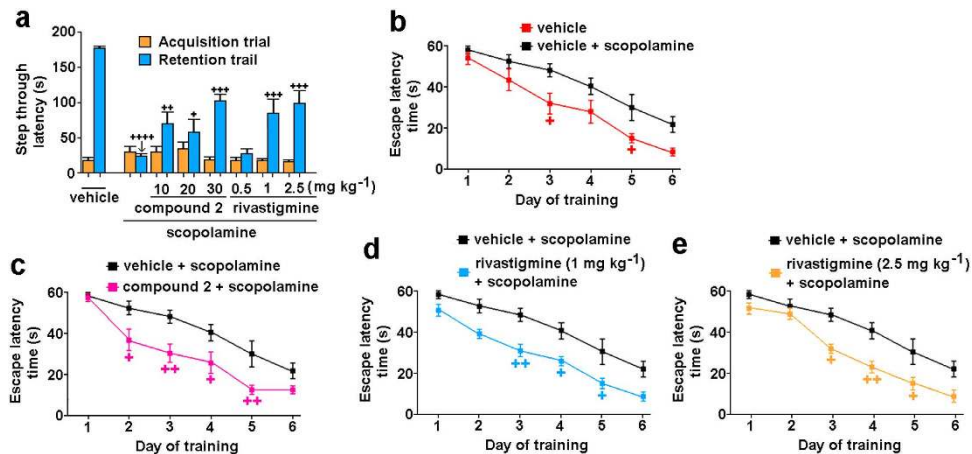


Figure 6. Effects of compound 2 and rivastigmine on scopolamine-induced memory impairment in the passive avoidance (a) and the Morris water maze tasks (b–e). (a) Data are mean step-through latencies \pm SEM ($n = 9$ –10 mice per group). Significance: $^+p < 0.05$; $^{++}p < 0.01$; $^{+++}p < 0.001$; $^{++++}p < 0.001$, versus scopolamine-treated control (in the retention phase). (b–e) Learning curves showing acquisition phase for vehicle-treated mice and scopolamine-treated control mice (b), scopolamine-treated control mice and scopolamine-induced memory-impaired mice treated with 30 mg kg⁻¹ compound 2 (c), or 1 mg kg⁻¹ (d) or 2.5 mg kg⁻¹ (e) rivastigmine. Data are mean escape latency \pm SEM from four daily trials. Significance versus scopolamine-treated control: $^+p < 0.05$; $^{++}p < 0.01$.

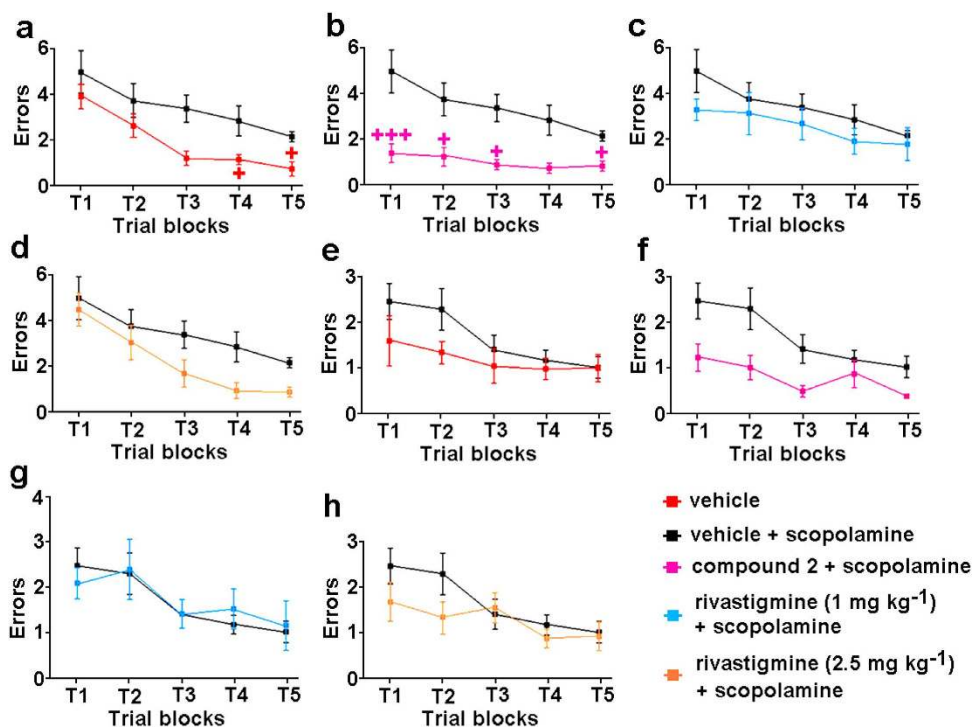


Figure 7. Effects of compound 2 and rivastigmine on scopolamine-induced memory impairment in the two-day radial arm water maze task. Spatial learning deficits expressed as mean number of errors \pm SEM in 15 trials in five blocks (T1–T5) of three trials on day 1 (a–d) and day 2 (e–h) of the RAWM task. Vehicle-treated mice and scopolamine-treated control mice (a,f), scopolamine-treated control mice and scopolamine-induced memory-impaired mice treated with 30 mg kg⁻¹ compound 2 (b,f), or 1 mg kg⁻¹ (c,g) or 2.5 mg kg⁻¹ (d,h) rivastigmine. Significance versus scopolamine-treated control mice: $^+p < 0.05$; $^{+++}p < 0.001$.

the mice treated with scopolamine and 2.5 mg kg⁻¹ rivastigmine travelled 3.64 m and 1.74 m on days 3 and 5, respectively. This effect was also observed at the lower treatment of 1 mg kg⁻¹ rivastigmine (day 3, 4.62 m; day 5, 1.58 m). The mean speed of the swimming was also determined to exclude any underlying sensorimotor deficits

in the animals treated with compound **2** and rivastigmine⁵². Compound **2** did not reduce the mean speed of swimming (vehicle, 0.17 m s⁻¹; scopolamine, 0.15 m s⁻¹; scopolamine + compound **2**, 0.16 m s⁻¹), although rivastigmine decreased it (1 mg kg⁻¹, 0.15 m s⁻¹; 2.5 mg kg⁻¹, 0.12 m s⁻¹).

Two-day radial arm water maze task. The radial arm water maze (RAWM) learning and memory task is a common method used to study memory deficits in mice, and it combines the spatial complexity of the dry radial arm with the rapid learning and strong motivation observed in the MWM^{53,54}. In this task incorrect arm entries (i.e., errors) are counted. The vehicle-treated mice had a mean of 4 errors during the first trial block, but <1 error by the end of the first day (Fig. 7a). In comparison, by the end of the five blocks of trials, the scopolamine-treated mice had a mean of nearly 3 errors (Fig. 7a). Mice treated with scopolamine and either compound **2** (30 mg kg⁻¹) (Fig. 7b) or rivastigmine (2.5 mg kg⁻¹) (Fig. 7d) all finished the acquisition phase making <1 error. Of note, the dose of 1 mg kg⁻¹ rivastigmine was not effective in this task (Fig. 7c,g). At the end of day two, all of the experimental groups completed the RAWM task with a mean performance of 1 error, with the exception of the mice treated with scopolamine and compound **2**, which showed better performance than the other groups, by making <1 error in the last trial block (Fig. 7e–h).

In-vivo safety profile of compound 2. To determine the *in-vivo* safety profile of compound **2** and properly interpret the results obtained in all three behavioural tasks, the impact of this inhibitor on motor coordination, sensorimotor functions and locomotor activity was determined. The effects of 30 mg kg⁻¹ and 100 mg kg⁻¹ compound **2** on motor coordination were tested with the rotarod test (Supplementary Methods). Here, compound **2** had no impact on the motor coordination of the mice, as it did not induce motor deficits, even at 100 mg kg⁻¹ (Supplementary Table 9). Also, after administration of compound **2**, there were no acute cholinergic adverse effects in the mice, even at 100 mg kg⁻¹ compound **2**. Any underlying sensorimotor deficits in the animals treated with compound **2** have also been excluded, as it did not reduce the mean speed of swimming in the MWM task (see Chapter “*Morris water maze task*”). Therefore, the observed transient reduction in the locomotor activity of mice (Supplementary Figure 9) did not appear to have any relevant impact on the data obtained in the learning and memory tests.

Discussion

Using the previously reported huBChE inhibitor as a starting point, a comprehensive series of 41 new sulfonamide analogs were designed and synthesized. Five types of inhibitors were developed that showed nanomolar to micromolar inhibition of huBChE. See Supplementary Discussion for details regarding the structure–activity relationships of the complete series of inhibitors and the discussion regarding other sulfonamide ChE inhibitors. The solved crystal structures of complexes with three inhibitors revealed their binding modes and represent an excellent basis for their further structure-based optimization. A thorough biological evaluation of our most potent inhibitor **2** revealed that this compound inhibits BChE activity on rat brain slices, is not cytotoxic and protects neuronal cells from toxic A β -species. *In-vitro* Caco-2 cell permeability of compound **2** can be classified as “good” according to the biopharmaceutical classification system of drug permeability. This compound is also highly plasma protein bound, has a half-life in human plasma longer than 2 hours, and its metabolic stability in cryopreserved hepatocytes is comparable to flurazepam and naloxone. Furthermore, compound **2** permeates into the brain of rats and we assume that its relatively modest brain-to-plasma ratio is actually quite good considering its molecular weight.

Since test animals with an increased brain BChE/AChE enzymatic activity ratio are currently not available, animals with an unaltered brain BChE/AChE enzymatic activity ratio (CD-1 Krf and C57BL/6J mice) were used. Procognitive properties of compound **2**, which targets the cholinergic system (BChE), were evaluated in an *in-vivo* model relevant to its mode of action. Scopolamine-induced amnesia was chosen since it is a model related to the cholinergic deficit that characterizes AD and is used in AD research for preclinical evaluation of cholinomimetics (compounds having an action similar to that of ACh)⁵⁵ e.g., ChE inhibitors^{55–59}. This model is useful for the evaluation of cognition-enhancing properties of ChE inhibitors without the risk of these drugs counteracting with the mechanism of the model^{56–59}. Scopolamine, a non-selective muscarinic ACh receptor antagonist is administered to test subjects to induce blockade of muscarinic ACh receptors in the central nervous system^{60,61} and produce cholinergic hypofunction at the pathophysiological level, and memory and cognitive deficits at the behavioural level⁵⁵. Scopolamine thus produces memory and cognitive deficits comparable to those caused by the cholinergic hypofunction in AD^{60,61}. Procognitive effects of ChE inhibitors in scopolamine-induced amnesia are the result of increased brain levels of ACh. ChE inhibitors interfere with the breakdown of ACh and cause its accumulation in the synapse, which then displaces scopolamine from muscarinic ACh receptors, and thus ameliorates the scopolamine-induced memory and cognitive deficits^{60,62}.

The dose of scopolamine used to model cholinergic deficit varies among studies, with a range from 0.2 mg kg⁻¹ to 2 mg kg⁻¹, depending on the behavioral assay or drug considered. In the present study, 1 mg kg⁻¹ scopolamine was injected IP before the acquisition trial of each test. This resulted in clear learning impairments in the negative controls used for the three behavioral tests performed. The anti-AD drug rivastigmine, which served as the positive control in these *in-vivo* assays, was used at concentrations comparable to those used in the clinic⁶³. This selection was justified by the literature data that indicate that treatments with >2.5 mg kg⁻¹ rivastigmine provide less ameliorating effects on scopolamine-induced cognitive deficits than those <2.5 mg kg⁻¹^{63,64} while also producing significant adverse effects, including hypersalivation, intestinal hyperperistalsis, and muscle cramps (i.e., tremor and retraction of the hindlimbs)⁶³.

Three behavioral tests were performed to determine whether compound **2** can attenuate the effects of scopolamine by increasing brain levels of ACh through selective BChE inhibition: the PA task, the MWM, and

the two-day RAWM tasks. These behavioral tests and their various modifications have been used recently to model human cognition⁶⁵. Details regarding these tests and their interpretation are given in the Methods and Supplementary Methods. The results of all three behavioral tasks performed *in-vivo* show that selective reversible BChE inhibition with compound **2** improved the memory, cognitive functions, and learning abilities of scopolamine-treated mice with an unaltered brain BChE/AChE enzymatic activity ratio. Compound **2** would thus be even more effective in alleviating symptoms caused by cholinergic hypofunction in advanced AD, in which brain BChE enzymatic activity is increased. The results also show that despite its relatively modest brain-to-plasma ratio, enough compound **2** partitions into the brain to ameliorate the induced memory and cognitive deficits.

As inhibition of ChEs in the basal ganglia, peripheral nervous system, and parasympathetic autonomic nervous system results in an excess of ACh, which is the basis for the adverse side effects of approved drugs for the treatment of patients with AD¹³, it was imperative to determine the *in-vivo* safety profile of compound **2**. We found no effects of compound **2** on motor coordination when tested with the rotarod test, no sensorimotor deficits in MWM task, and no acute cholinergic adverse effects in the mice, even at 100 mg kg⁻¹. The combination of these properties makes compound **2** an advanced lead compound for developing drugs for alleviating symptoms caused by cholinergic hypofunction in advanced AD, in which brain BChE enzymatic activity is increased. Additionally, compound **2** is a powerful molecular tool to study BChE biology and to validate its potential as a therapeutic target.

Methods

Chemistry. Only the syntheses of the most potent **type I–V** inhibitors (i.e., compounds **2**, **3**, **4**, **5**, **6**) are described in this section. Those for all of the novel compounds are described in the Supplementary Methods.

Synthesis of intermediates. The syntheses of intermediates **9**, **10**, **11**, and **12** (see Supplementary Figures 1, 2, 3, and 5) were achieved according to the relevant literature procedures^{28,66}.

General procedure for the synthesis of 2, 5, and 6 (see Supplementary Figures 2, 3, and 5). Amine **10**, **11**, or **12** (1.0 equiv.) was dissolved in dichloromethane (DCM) and cooled to 0 °C. The reaction mixture was stirred, and Et₃N (1.0 equiv.) was added drop-wise. After 15 min, naphthalene-2-sulfonyl chloride (1.0 equiv.) was added, and the reaction mixture was allowed to warm up to room temperature and then stirred for 24 h. The reaction mixture was next transferred into a separating funnel, washed with water, followed by saturated aqueous NaHCO₃ solution, dried over anhydrous Na₂SO₄, and evaporated. The crude product was purified by flash column chromatography using a suitable solvent system as the eluent (see Supplementary Methods), to yield pure **2** (1.654 g, 90%), **5** (1.565 g, 87%), and **6** (0.254 g, 86%).

General procedure for the synthesis of 3 and 13 (see Supplementary Figure 1). Compound **10** (1.0 equiv.) was suspended in DCM and cooled to 0 °C. The reaction mixture was stirred, and Et₃N (3.0 equiv.) was added drop-wise. After 15 min, naphthalene-2-sulfonyl chloride (1.0 equiv.) or 3-nitrobenzene-1-sulfonyl chloride (1.0 equiv.) was added, and the reaction mixture was allowed to warm up to room temperature and then stirred for 24 h. The reaction mixture was next transferred into a separating funnel, washed with water, followed by saturated aqueous NaHCO₃ solution, dried over anhydrous Na₂SO₄, and evaporated. The crude product was purified by flash column chromatography using a suitable solvent system as the eluent (see Supplementary Methods) to yield pure **3** (0.220 g, 93%) and **13** (0.145 g, 40%).

Synthesis of 4 (see Supplementary Figure 1). Aromatic nitro compound **13** (0.120 g, 0.253 mmol, 1.0 equiv.) was dissolved in a mixture of tetrahydrofuran (THF)/MeOH (1:1, v/v) and cooled to 0 °C. NiCl₂ × 6H₂O (0.241 g, 1.012 mmol, 4.0 equiv.) and NaBH₄ (0.172 g, 4.554 mmol, 18.0 equiv.) were added, and the resulting suspension was stirred at 0 °C for 2 h, and then allowed to warm up to room temperature, and stirred for an additional 16 h. The solvent was evaporated and DCM (15 mL) was added to the residue. The precipitated solid was filtered under suction, and washed with DCM (15 mL). The combined filtrates were evaporated, and the crude product purified by flash column chromatography using DCM/MeOH (20:1, v/v) as the eluent, to produce 0.064 g of **4** as a pale brown solid (57% yield).

For the inhibition of BChE in the rat brain slices, the *in-vitro* cytotoxicity assay, the *in-vivo* blood plasma to brain distribution assay, and the *in-vivo* activity assays, compound **2** was used in the form of its hydrochloride salt (see Supplementary Scheme S2, Supplementary Methods). All of the novel compounds were appropriately characterized and were of high purity (>95%; analytical HPLC, Supplementary Methods).

Biology. *In-vitro* inhibitory activity against the ChEs. The inhibitory potencies of the compounds against the ChEs were determined using the method of Ellman³². The assay protocol and IC₅₀ calculations are described in the Supplementary Methods.

Kinetic studies for huBChE inhibition. The mode of action of huBChE inhibition by pure enantiomers of compound **2** was determined as previously described²⁸. Briefly, the time-course of yellow color formation was followed on a Bio-logic SFM-2000 stopped flow apparatus at 25 °C. The two buffer solutions were prepared as one that contained the substrate butyrylthiocholine iodide, the 5,5'-dithiobis (2-nitrobenzoic acid) reagent (Ellman reagent), and test compound **2** (each pure enantiomer), and the other that contained huBChE. The buffer solutions were injected into a mixing chamber using syringes. The resulting solution contained 44 μM butyrylthiocholine iodide, 1 mM Ellman reagent, 8.2 nM huBChE, 50 nM test compound, and 0.007 M DMSO (i.e., 0.05% v/v). The absorbance was followed immediately at 412 nm, and until the change reached zero. The progress curves

obtained were analyzed simultaneously, using the ENZO application³⁶, which can derive and numerically solve a system of differential equations, and fit their coefficients. Several reaction mechanisms were tested. The simplest one for the reproduction of the progress curves in the absence and presence of (+)-2 and (–)-2 was chosen, and the corresponding inhibition constants were determined. The results file can be accessed by loading the ENZO project ID <http://enzo.cmm.ki.si/kinetic.php?uwd=151006561&load=true>, selecting the 'Set Parameters' tab, and pressing 'Start'.

Crystallization, data collection, and processing. Crystallization, data collection, and processing are described in Supplementary Methods.

Cell culture and treatments. The HepG2 cell line was obtained from American Type Culture Collection (LGC Standards, UK) and was cultured in RPMI 1640 medium (Sigma-Aldrich, St. Louis/MO, USA) supplemented with 10% fetal bovine serum (Gibco, Grand Island/NY, USA), 2 mM L-glutamine, 100 U mL⁻¹ penicillin and 100 µg mL⁻¹ streptomycin (all from Sigma-Aldrich) in a humidified chamber at 37 °C and 5% CO₂. Compound 2 was used at 0.625 µM to 125 µM, in DMSO.

Human neuroblastoma SH-SY5Y cells were obtained from American Type Culture Collection (CRL-2266, Manassas, VA, USA). They were grown in Dulbecco's modified Eagle's medium (Sigma, St. Louis, MO) supplemented with 10% fetal bovine serum (HyClone, Logan, UT, USA), 2 mM L-glutamine, 50 U mL⁻¹ penicillin and 50 µg mL⁻¹ streptomycin (Sigma, St. Louis, MO, USA), in a humidified atmosphere of 95% air and 5% CO₂ at 37 °C, and grown to 80% confluence. Prior to cell treatments, complete medium was replaced with reduced-serum medium (i.e., with 2% fetal bovine serum). Compound 2 was prepared as a stock solution of 10 mM in DMSO and was used at concentrations of 1 µM to 100 µM. For the cytotoxic stimuli, Aβ_(1–42) was dissolved in DMSO to give a 1 mM stock solution and 24 h prior cell treatment, the peptide was incubated at final concentration of 5 µM in reduced-serum medium in the absence and presence of compound 2 (1–10 µM) at 37 °C, to induce Aβ aggregation. The metabolic activity and cell viability assays and the assessment of cytotoxicity are described in Supplementary Methods.

Aβ_(1–42) aggregation inhibitory activity. The thioflavin-T (ThT) fluorometric and dot-blot assays used are described in Supplementary Methods.

Inhibition of BChE in rat brain slices. **Animals.** Adult male Wistar rats (500–600 g; The Wistar Institute, Philadelphia, PA, USA) were used in this study. The rats were handled according to the European Community Council Directive of 23 November 1986 (86/609/EEC), and the National Veterinary Institute guide for the Care and Use of Laboratory Animals. All efforts were made to minimize the number of rats used and their suffering.

Preparation of brain tissue. The rats were sacrificed by decapitation under CO₂ anesthesia. The brain of each animal was rapidly removed and immediately frozen on dry-ice powder, wrapped in Parafilm to prevent desiccation, and stored at –80 °C. Before cutting, the brains were allowed to equilibrate with the temperature of the cryostat chamber that had been adjusted to –20 °C. Brains were cut into 16 serial sections of 20 µm thickness in a coronal plane on a Leica SM2000R microtome with a Physitemp freezing stage and a BFS-30TC controller. The cytoarchitectonic parcellation of the brain areas was guided by the atlas of the adult rat brain by Paxinos and Watson⁶⁷. Each section was thaw-mounted onto an RNase-free glass slide coated with a 0.01% solution of (poly)L-lysine in dimethylpyrocarbonate, fixed for 5 min in 4% paraformaldehyde, and rinsed (3 × 3 min) in phosphate-buffered saline (PBS) with potassium. Sections were stained for BuChE or AChE using histochemical techniques³⁷. The ChE histochemistry and the analysis of BuChE staining of brain structures were as described in the Supplementary Methods.

In-vitro pharmacokinetic of compound 2. Caco-2 monolayer bidirectional permeability assay is described in detail in the Supporting Methods. In solution properties, *in vitro* metabolism assays, and identification and characterization of metabolites of compound 2 (in the form of its hydrochloride salt) when incubated with cryopreserved human hepatocytes were performed by Eurofins Panlab (St. Charles, MO, USA), in study no. 100028035. In each experiment the respective reference compounds were tested concurrently with test compound 2 and the data were compared with historical values determined at Eurofins. The experiment was accepted in accordance with Eurofins validation Standard Operating Procedure. Details on these experiments are described in the Supporting Information.

In-vivo blood plasma to brain distribution. **Animals.** The blood plasma–brain distribution of compound 2 was measured in 3-month-old female Wistar Han rats with body weight of 220 g ± 10%. The rats were handled according to the European Community Council Directive of 23 November 1986 (86/609/EEC), and the National Veterinary Institute guide for the Care and Use of Laboratory animals. The experimental design was evaluated by the National Ethical Committee for Animal Experimentation and approved by the Veterinary Administration of the Republic of Slovenia. All efforts were made to minimize the number of rats used and their suffering.

Chemicals used in the BBB assay. Here, 10 mg mL⁻¹ compound 2 was dissolved in 1% Tween 80 isotonized with sodium chloride, and sterilized by filtration. Isotonized 1% Tween 80 was used as the negative control, and 2 mg mL⁻¹ donepezil in the same solution was used as the positive control.

In-vivo blood plasma–brain distribution assay protocol, sample collection and work up. Four rats were given compound 2 and three rats were used for each of the positive and negative controls. The IP injected doses of

compound **2** and donepezil were 10 mg kg^{-1} and 2 mg kg^{-1} , respectively. The rats were euthanized by CO_2 inhalation 1 h after administration of compound **2**. Immediately, 2 mL blood was collected in Vacutainer tubes with $10.8 \text{ mg K}_2\text{EDTA}$, and the brain tissue was isolated. Blood plasma was obtained after centrifugation of the blood at $3,500 \text{ rpm}$ for 10 min. The blood plasma and brain tissue were stored at -20°C until further sample preparation.

Four aliquots of approximately 150 mg of each brain tissue sample were weighted and homogenized in 2-mL microcentrifuge tubes (Eppendorf, Germany) with $25 \mu\text{L}$ internal standard solution ($450 \mu\text{g L}^{-1}$ haloperidol in 80% MeOH with 0.1% acetic acid), $300 \mu\text{L}$ PBS, and $125 \mu\text{L}$ methanol, in a blender (Bullet Blender; Next Advance, NY, USA) for 3 min at speed setting '8' with 0.5-mm glass beads. The homogenate was centrifuged at $10,000 \text{ rpm}$ for 7 min, and the supernatant was removed. The sample was mixed again in the blender for 1 min at speed setting '5', and a second supernatant was collected after centrifugation as before. These supernatants were then combined, and $900 \mu\text{L}$ 2% H_3PO_4 was added prior to solid phase extraction (SPE).

Blood plasma aliquots ($150 \mu\text{L}$) in 2-mL microcentrifuge tubes (Eppendorf) were mixed with $25 \mu\text{L}$ internal standard solution ($450 \mu\text{g L}^{-1}$ haloperidol in 80% MeOH with 0.1% acetic acid), $300 \mu\text{L}$ PBS and $125 \mu\text{L}$ MeOH. The samples were mixed in the blender for 1 min at minimum speed, and sonicated in an ultrasound bath for 5 min. Then $900 \mu\text{L}$ 2% H_3PO_4 was added in two aliquots during the quantitative sample transfer to the SPE column.

For the preparation of all of the samples for LC-MS/MS quantification, Bond Elut Plexa PCX (30 mg, 3 mL) SPE columns were used. The SPE columns were conditioned with 2 mL methanol and equilibrated with 2 mL water before the samples were slowly loaded. Then 2 mL 2% formic acid, followed by 2 mL MeOH/MeCN mixture (1:1, v/v) were used for column washing. The samples were eluted with 1 mL 25% ammonia in water/MeOH/MeCN (1:2:2, v/v), and dried for 20 min in a concentration evaporator (Turbovap) at 60°C . The dried samples were stored at -20°C until analysis. The samples were reconstituted in $200 \mu\text{L}$ 0.1% acetic acid in 80% MeOH using 2×2 -min mixing in the blender at minimum speed, separated by a 10-min waiting interval.

For the calculation of the brain-to-plasma ratio of compound **2** its concentration in the brain which is given in $\mu\text{g kg}^{-1}$ and its concentration in blood plasma which is given in $\mu\text{g L}^{-1}$ the specific density of wet rat brain (1.05 g mL^{-1}) was used⁶⁸. LC-MS/MS analysis and LC-MS/MS method validation are described in the Supplementary Methods.

In-vivo activity assays. **Animals.** Eight-week-old male Albino Swiss (CD-1 Krf) mice weighing from 18 g to 22 g were used in the passive avoidance task, and the locomotor activity and rotarod tests, and C57BL/6J mice of the same age were used in the MWM and the RAWM tasks. The mice were housed in groups of 10 per cage at room temperature ($22 \pm 2^\circ\text{C}$) under a light/dark (12 h:12 h) cycle. The mice had free access to food and water, and the ambient temperature and humidity of the room were kept constant throughout all of the tests. For the behavioral tasks, the mice were selected at random, and each group consisted of 8 to 10 mice dose^{-1} . The experiments were performed between 08:00 and 14:00. Immediately after these *in-vivo* assays, the animals were euthanized by cervical dislocation. The maintenance and treatment of the laboratory animals were carried out in full accordance with the guidelines issued by the Local Ethics Committee of the Jagiellonian University in Krakow (ZI/862/2013). All efforts were made to minimize the number of mice used and their suffering.

Chemicals used in the in-vivo activity assays. For the *in-vivo* experiments, compound **2** was suspended in 1% Tween 80 (Polskie Odczynniki Chemiczne, Poland), with IP injections 60 min before the acquisition trial of learning and memory tasks, and the locomotor activity and rotarod tests. Rivastigmine hydrogen tartrate was from Sigma Aldrich (Poland), and it was dissolved in distilled water and administered by the same route as compound **2**. Control mice were given an appropriate amount of vehicle (1% Tween 80, IP). (–)-Scopolamine hydrobromide was from Sigma Aldrich (Poland). To induce memory impairment, scopolamine was dissolved in distilled water, with IP administration at 1 mg kg^{-1} 30 min before the acquisition trial of each learning and memory task. Vehicle-treated mice were used as the negative control. For comparison, the same experiments were performed in mice similarly treated with scopolamine and the anti-AD drug rivastigmine, which served as the positive control in these *in-vivo* assays. The behavioral testing paradigms are described in the Supplementary Methods.

References

1. Querfurth, H. W. & LaFerla, F. M. Alzheimer's disease. *N. Engl. J. Med.* **362**, 329–344 (2010).
2. Glabe, C. C. In *Alzheimer's Disease: Cellular and Molecular Aspects of Amyloid β 1st edn* Ch. 8 (eds Harris, J. R. & Fahrenholz, F.) 167–177 (Springer, 2005).
3. Elsinghorst, P. W., Härtig, W., Goldhammer, S., Grosche, J. & Gütschow, M. A Gorge-spanning, high-affinity cholinesterase inhibitor to explore β -amyloid plaques. *Org. Biomol. Chem.* **7**, 3940–3946 (2009).
4. Morris, M. *et al.* Tau post-translational modifications in wild-type and human amyloid precursor protein transgenic mice. *Nat. Neurosci.* **18**, 1183–1189 (2015).
5. Scherder, E. In *Aging and Dementia: Neuropsychology, Motor Skills, and Pain 1st ed.* Ch. 1, 9–32 (VU University Press, 2011).
6. Scarpini, E., Schelterns, P. & Feldman, H. Treatment of Alzheimer's disease: current status and new perspectives. *Lancet Neurol.* **2**, 539–547 (2003).
7. Perry, E. K. *et al.* Correlation of cholinergic abnormalities with senile plaques and mental test scores in senile dementia. *Br. Med. J.* **2**, 1457–1459 (1978).
8. Reid, G. A., Chilukuri, N. & Darvesh, S. Butyrylcholinesterase and the cholinergic system. *Neuroscience* **234**, 53–68 (2013).
9. Giacobini, E. In *Treatment of Dementia: A New Generation of Progress 1st edn* Ch. 2 (eds Meyer, E. M., Simpkins, J. W., Yamamoto, J. & Crews, F. T.) 19–34 (Springer, 1992).
10. Sugimoto, H., Iimura, Y., Yamanishi, Y. & Yamatsu, K. Synthesis and structure-activity relationships of acetylcholinesterase inhibitors: 1-benzyl-4-[(5,6-dimethoxy-1-oxindan-2-yl)methyl]piperidine hydrochloride and related compounds. *J. Med. Chem.* **38**, 4821–4829 (1995).
11. Greenblatt, H. M., Kryger, G., Lewis, T., Silman, I. & Sussman, J. L. Structure of acetylcholinesterase complexed with (–)-galanthamine at 2.3 Å resolution. *FEBS Lett.* **463**, 321–326 (1999).

12. Bar-On, P. *et al.* Kinetic and structural studies on the interaction of cholinesterases with the anti-Alzheimer drug rivastigmine. *Biochemistry* **41**, 3555–3564 (2002).
13. Hartmann, J. *et al.* Excessive hippocampal acetylcholine levels in acetylcholinesterase-deficient mice are moderated by butyrylcholinesterase activity. *J. Neurochem.* **100**, 1421–1429 (2007).
14. Ballard, C., Greig, N., Guillozet-Bongaarts, A., Enz, A. & Darvesh, S. Cholinesterases: roles in the brain during health and disease. *Curr. Alzheimer Res.* **2**, 307–318 (2005).
15. Wilkinson, D. G., Francis, P. T., Schwam, E. & Payne-Parrish, J. Cholinesterase inhibitors used in the treatment of Alzheimer's disease: The relationship between pharmacological effects and clinical efficacy. *Drugs Aging* **21**, 453–478 (2004).
16. Hansen, R. A. *et al.* Efficacy and safety of donepezil, galantamine, and rivastigmine for the treatment of Alzheimer's disease: A systematic review and meta-analysis. *Clin. Inter. Aging* **3**, 211–225 (2008).
17. Mesulam, M. M. *et al.* Acetylcholinesterase knockouts establish central cholinergic pathways and can use butyrylcholinesterase to hydrolyze acetylcholine. *Neuroscience* **110**, 627–639 (2002).
18. Li, B., Duysen, E. G., Carlson, M. & Lockridge, O. The butyrylcholinesterase knockout mouse as a model for human butyrylcholinesterase deficiency. *J. Pharmacol. Exp. Ther.* **324**, 1146–1154 (2008).
19. Greig, N. H. *et al.* Selective butyrylcholinesterase inhibition elevates brain acetylcholine, augments learning and lowers Alzheimer β -amyloid peptide in rodent. *Proc. Natl. Acad. Sci.* **102**, 17213–17218 (2005).
20. Summers, W. K., Majovski, L. V., Marsh, G. M., Tachiki, K. & Kling, A. Oral tetrahydroaminoacridine in long-term treatment of senile dementia, Alzheimer type. *N. Engl. J. Med.* **315**, 1241–1245 (1986).
21. Decker, M. Homobivalent quinazolinimines as novel nanomolar inhibitors of cholinesterase with dirigible selectivity towards butyrylcholinesterase. *J. Med. Chem.* **49**, 5411–5413 (2006).
22. Rizzo, S. *et al.* Benzofuran-based hybrid compounds for the inhibition of cholinesterase activity, β amyloid aggregation, and A β neurotoxicity. *J. Med. Chem.* **51**, 2883–2886 (2008).
23. Darvesh, S. *et al.* Carbamates with differential mechanism of inhibition toward acetylcholinesterase and butyrylcholinesterase. *J. Med. Chem.* **51**, 4200–4212 (2008).
24. Carolan, C. G. *et al.* Isosorbide-2-benzyl carbamate-5-salicylate, a peripheral anionic site binding subnanomolar selective butyrylcholinesterase inhibitor. *J. Med. Chem.* **53**, 1190–1199 (2010).
25. Zha, X. *et al.* Novel tacrine-benzofuran hybrids as potent multitarget-directed ligands for the treatment of Alzheimer's disease: design, synthesis, biological evaluation, and X-ray crystallography. *J. Med. Chem.* **59**, 114–131 (2016).
26. Bartolucci, C., Stojan, J., Yu, Q., Greig, N. H. & Lamba, D. Kinetics of Torpedo californica acetylcholinesterase inhibition by bisnorcymserine and crystal structure of the complex with its leaving group. *Biochem. J.* **444**, 269–277 (2012).
27. Copeland, R. A. In *Evaluation of Enzyme Inhibitors in Drug Discovery: A Guide for Medicinal Chemists and Pharmacologists* 1st ed. Ch. 8, 214–248 (John Wiley & Sons, 2005).
28. Singh, J., Petter, R. C., Baillie, T. A. & Whitty, A. The resurgence of covalent drugs. *Nat. Rev. Drug Discov.* **10**, 307–317 (2011).
29. Brus, B. *et al.* Discovery, biological evaluation, and crystal structure of a novel nanomolar selective butyrylcholinesterase inhibitor. *J. Med. Chem.* **57**, 8167–8179 (2014).
30. Lipinski, C. A., Lombardo, F., Dominy, B. W. & Feeney, P. J. Experimental and computational approaches to estimate solubility and permeability in drug discovery and development settings. *Adv. Drug Deliv. Rev.* **46**, 3–26 (2001).
31. Ciapetti, P. & Giethlen, B. In *The Practice of Medicinal Chemistry* 3rd edn Ch. 15 (ed. Wermuth, C. G.) 290–342 (Academic Press, 2008).
32. Ellman, G. L., Courtney, K. D., Andres, jr. V. & Featherstone, R. M. A new and rapid colorimetric determination of acetylcholinesterase activity. *Biochem. Pharmacol.* **7**, 88–95 (1961).
33. Kryger, G. *et al.* Structures of recombinant native and E202Q mutant human acetylcholinesterase complexed with the snake-venom toxin fasciculin-II. *Acta Crystallogr. D Biol. Crystallogr.* **56**, 1385–1394 (2000).
34. Stojan, J. *et al.* Concentration-dependent reversible activation-inhibition of human butyrylcholinesterase by tetraethylammonium ion. *Eur. J. Biochem.* **269**, 1154–1161 (2002).
35. Copeland, R. A. In *Evaluation of Enzyme Inhibitors in Drug Discovery: A Guide for Medicinal Chemists and Pharmacologists* 2nd ed. Ch. 7, 245–285 (John Wiley & Sons, 2013).
36. Bevc, S. *et al.* ENZO: A web tool for derivation and evaluation of kinetic models of enzyme catalyzed reactions. *PLoS One* **6**, e22265 (2011).
37. Ramesh, V. V. E. *et al.* Carboxamide versus sulfonamide in peptide backbone folding: a case study with a hetero foldamer. *Org. Lett.* **15**, 1504–1507 (2013).
38. Koelle, G. B. & Friedenwald, J. A. A histochemical method for localizing cholinesterase activity. *Proc. Soc. Exp. Biol. Med. Soc. Exp. Biol. Med.* **70**, 617–622 (1949).
39. Darvesh, S., Grantham, D. L. & Hopkins, D. A. Distribution of butyrylcholinesterase in the human amygdala and hippocampal formation. *J. Comp. Neurol.* **393**, 374–390 (1998).
40. Geula, C. & Nagykerly, N. Butyrylcholinesterase activity in the rat forebrain and upper brainstem: postnatal development and adult distribution. *Exp. Neurol.* **204**, 640–657 (2007).
41. Giordano, C. R., Terlecky, L. J., Bollig-Fischer, A., Walton, P. A. & Terlecky, S. R. Amyloid-beta neuroprotection mediated by a targeted antioxidant. *Sci. Rep.* **4**, 1–9 (2014).
42. Rankovic, Z. CNS drug design: balancing physicochemical properties for optimal brain exposure. *J. Med. Chem.* **58**, 2584–2608 (2015).
43. Hubatsch, I., Ragnarsson, E. G. E. & Artursson, P. Determination of drug permeability and prediction of drug absorption in Caco-2 monolayers. *Nat. Protoc.* **2**, 2111–2119 (2007).
44. Sun, H., Chow, E. C., Liu, S., Du, Y. & Pang, K. S. The Caco-2 cell monolayer: Usefulness and limitations. *Expert Opin. Drug. Metab. Toxicol.* **4**, 395–411 (2008).
45. Žakelj, S., Berginc, K., Roškar, R., Kraljič, B. & Kristl, A. Do the recommended standards for *in vitro* biopharmaceutical classification of drug permeability meet the “passive transport” criterion for bioavaives? *Curr. Drug Metab.* **14**, 21–27 (2013).
46. Di, L. & Kerns, E. H. Transporter Methods. In *Drug-Like Properties: Concepts, Structure, Design, and Methods from ADME to Toxicity Optimization* 2nd edn Ch. 27, 339–350 (Academic Press, 2016).
47. Fesce, R. & Fumagalli, G. Drug Distribution and Elimination. In *General and Molecular Pharmacology: Principles of Drug Action* 1st edn Ch. 5, (eds Clementi, F. & Fumagalli, G.) 45–60 (Wiley, 2015).
48. Geerts, H. *et al.* Brain levels and acetylcholinesterase inhibition with galantamine and donepezil in rats, mice, and rabbits. *Brain Res.* **1033**, 186–193 (2005).
49. Gulcan, H. O. *et al.* Design, synthesis and biological evaluation of novel 6H-benzo[c]chromen-6-one, and 7,8,9,10-tetrahydro-benzo[c]chromen-6-one derivatives as potential cholinesterase inhibitors. *Bioorg. Med. Chem.* **22**, 5141–5154 (2014).
50. Patil, S. S., Sunyer, B., Höger, H. & Lubec, G. Evaluation of spatial memory of C57BL/6j and CD1 mice in the Barnes maze, the Multiple T-maze and in the Morris water maze. *Behav. Brain Res.* **198**, 58–68 (2009).
51. Puzzo, D., Lee, L., Palmeri, A., Calabrese, G. & Arancio, O. Behavioral assays with mouse models of Alzheimer's disease: Practical considerations and guidelines. *Biochem. Pharmacol.* **88**(4), 450–467 (2014).
52. Vorhees, C. V. & Williams, M. T. Morris water maze: procedures for assessing spatial and related forms of learning and memory. *Nat. Protoc.* **1**, 848–858 (2006).

53. Alamed, J., Wilcock, D. M., Diamond, D. M., Gordon, M. N. & Morgan, D. Two-day radial-arm water maze learning and memory task; robust resolution of amyloid-related memory deficits in transgenic mice. *Nat. Protoc.* **1**, 1671–1679 (2006).
54. Sudduth, T. L., Weekman, E. M., Brothers, H. M., Braun, K. & Wilcock, D. M. β -amyloid deposition is shifted to the vasculature and memory impairment is exacerbated when hyperhomocysteinemia is induced in APP/PS1 transgenic mice. *Alzheimers Res. Ther.* **6**, 32 (2014).
55. Van Dam, D. & De Deyn, P. P. Drug discovery in dementia: the role of rodent models. *Nat. Rev. Drug Discov.* **5**, 956–970 (2006).
56. Bouger, P. C. & van der Staay, F. J. Rats with scopolamine- or MK-801-induced spatial discrimination deficits in the cone field task: animal models for impaired spatial orientation performance. *Eur. Neuropsychopharmacol.* **15**, 331–346 (2005).
57. van der Staay, F. J. & Bouger, P. C. Effects of the cholinesterase inhibitors donepezil and metrifonate on scopolamine-induced impairments in the spatial cone field orientation task in rats. *Behav. Brain Res.* **156**, 1–10 (2005).
58. Stemmelin, J., Cassel, J. C., Will, B. & Kelche, C. Sensitivity to cholinergic drug treatments of aged rats with variable degrees of spatial memory impairment. *Behav. Brain Res.* **98**, 53–66 (1999).
59. Vardigan, J. D. *et al.* Improved cognition without adverse effects: novel M1 muscarinic potentiator compares favorably to donepezil and xanomeline in rhesus monkey. *Psychopharmacology (Berl)*. **232**, 1859–1866 (2015).
60. Ebert, U. & Kirch, W. Scopolamine model of dementia: electroencephalogram findings and cognitive performance. *Eur. J. Clin. Invest.* **28**, 944–949 (1998).
61. Bajo, R. *et al.* Scopolamine effects on functional brain connectivity: a pharmacological model of Alzheimer's disease. *Sci. Rep.* **5**, 1–6 (2015).
62. Snyder, P. J., Bednar, M. M., Cromer, J. R. & Matuff, P. Reversal of scopolamine-induced deficits with a single dose of donepezil, an acetylcholine inhibitor. *Alzheimer's & Dementia* **1**, 126–135 (2005).
63. Zhang, W. W. *et al.* Peripheral cholinergic antagonist anisodamine counteracts cholinergic adverse effects and facilitates cognitive amelioration of rivastigmine. *J. Neural Transm. (Vienna)* **116**, 1643–1649 (2009).
64. Bejar, C., Wang, R. H. & Weinstock, M. Effect of rivastigmine on scopolamine-induced memory impairment in rats. *Eur. J. Pharmacol.* **383**, 231–240 (1999).
65. Zhang, J. *et al.* BZYX, a novel acetylcholinesterase inhibitor, significantly improved chemicals-induced learning and memory impairments on rodents and protected PC12 cells from apoptosis induced by hydrogen peroxide. *Eur. J. Pharmacol.* **613**, 1–9 (2009).
66. Košak, U., Brus, B. & Gobec, S. Straightforward synthesis of orthogonally protected piperidin-3-ylmethanamine and piperidin-4-ylmethanamine derivatives. *Tetrahedron Lett.* **55**, 2037–2039 (2014).
67. Paxinos, G. & Watson, C. In *The Rat Brain in Stereotaxic Coordinates* 2nd edn (Academic Press, 1986).
68. DiResta, G. R. *et al.* Measurement of Brain Tissue Density Using Pycnometry. In *Brain Edema VIII* 1st edn Ch. 12, (eds Reulen, H. J., Baethmann, A., Fenstermacher, J., Marmarou, A. & Spatz, M.) 34–36 (Springer, 2015).

Acknowledgements

This work was supported by the Slovenian Research Agency, the France-Alzheimer Foundation, the Agence Nationale de la Recherche (ANR), and Institut Français. We thank Marielle Vandhammer and Marie Trosvalet for providing us with lyophilized murine AChE and human BChE, as well as for continuous and fruitful discussions. We thank Domen Kutoša, Urša Jarc, Julija Lipušček, Aljoša Jelenko, Matevž Černigoj and Jure Breznik for their contributions. We thank Dr. Dušan Žigon (Jožef Stefan Institute, Ljubljana, Slovenia) for performing the mass spectrometry measurements. We also thank Dr. Chris Berrie for critical reading of the manuscript.

Author Contributions

U.K. participated in the design of the inhibitors, performed the chemistry, *in-vitro* ChE inhibition assays and chiral HPLC resolution. B.B. participated in the design of the inhibitors, performed *in-vitro* ChE inhibition assays, chiral HPLC resolution, inhibition kinetics studies, experiments on rat brain slices, and participated in the crystallographic studies. D.K. participated in the design of the inhibitors, performed the chemistry, *in-vitro* ChEs inhibition assays and the $A\beta_{(1-42)}$ aggregation inhibitory activity assays. R.Š. performed the chemistry. S.Ž. participated in the *in-vivo* blood plasma–brain distribution assay, performed the work up and the LC-MS/MS analysis of samples obtained in the *in-vivo* blood-brain barrier permeation assay and performed the *in-vitro* permeability assay with Caco2 cells. J.T. performed the work up and LC-MS/MS analysis of samples obtained in the *in-vivo* blood-brain barrier permeation assay. A.P. performed the cytotoxicity and neuroprotectivity assays with SH-SY5Y cells. J.Š. performed the cytotoxicity and neuroprotectivity assays with SH-SY5Y cells. M.G. performed the cytotoxicity assays with HepG2 cells. M.Ž. performed assays of inhibition of BChE on rat brain slices and the *in-vivo* blood plasma–brain distribution assays. L.T. performed *in vivo* blood plasma–brain distribution assays. M.P. performed *in vivo* blood plasma–brain distribution assays. K.S. performed and analyzed data from the *in-vivo* activity assays. A.P. participated in performance and analysis of the *in-vivo* activity assays. B.F. worked on the data from the *in-vivo* activity assays. F.N. prepared and purified the huBChE. X.B. prepared and purified the huBChE. A.W. participated in *in-vivo* activity assays. B.M. participated in *in-vivo* activity assays. J.S. performed inhibition kinetic studies. I.M.R. oversaw the cytotoxicity assays with HepG2 cells. J.K. oversaw the cytotoxicity and neuroprotectivity assays with SH-SY5Y cells. N.C. performed crystallographic studies. J.P.C. oversaw the crystallographic studies. S.G. conceived and oversaw the project. All of the authors contributed to the design, analysis and discussion of the research and the writing of the manuscript.

Additional Information

Supplementary information accompanies this paper at <http://www.nature.com/srep>

Competing financial interests: The authors declare no competing financial interests.

How to cite this article: Košak, U. *et al.* Development of an *in-vivo* active reversible butyrylcholinesterase inhibitor. *Sci. Rep.* **6**, 39495; doi: 10.1038/srep39495 (2016).

Publisher's note: Springer Nature remains neutral with regard to jurisdictional claims in published maps and institutional affiliations.



This work is licensed under a Creative Commons Attribution 4.0 International License. The images or other third party material in this article are included in the article's Creative Commons license, unless indicated otherwise in the credit line; if the material is not included under the Creative Commons license, users will need to obtain permission from the license holder to reproduce the material. To view a copy of this license, visit <http://creativecommons.org/licenses/by/4.0/>

© The Author(s) 2016